JOURNAL OF GUIDANCE, CONTROL, AND DYNAMICS
Vol. 29, No. 1, January–February 2006

Optimal Planner for Spacecraft Formations in Elliptical Orbits

Darren J. Zanon* and Mark E. Campbell†
Cornell University, Ithaca, New York 14853

An optimal planner for spacecraft formations in elliptical reference orbits is presented. A fast solution to an individual spacecraft minimum time or fuel maneuver using the Hamilton–Jacobi–Bellman formulation is developed using spline approximations to evaluate thrust effect integrals. The individual optimal spacecraft maneuvers use realistic low-thrust, bounded inputs similar to future electric propulsion systems. A formation optimal planner is then formulated using the individual spacecraft maneuvers as a basis. The formulation is easily scalable to larger clusters, provably optimal over the formation, and numerically robust; it also requires minimal communication between fleet members. An example is presented of a tetrahedron formation in a highly elliptical reference orbit ($e = 0.8$), with solutions to both formation minimum-time and minimum-fuel problems given. Comparison with linear programming techniques show a distinct savings in fuel usage for high-eccentricity examples.

I. Introduction

AUTONOMOUS satellite formations represent a key component in several ongoing and proposed NASA and Department of Defense projects.[1–4] These missions will require a variety of formations held under vastly differing orbital conditions. The advantages to such formations are an increase in scientific gains while potentially reducing costs and extending mission life. However, the technological challenges presented by this technique have been difficult to overcome: Fleetwide communication and fault detection, collision avoidance, and path planning and control are all active areas of exploration in the field.[5–7]

The planning and control problem is generally posed in two forms: formation maneuvering, in which the spacecraft plan and execute a thrust command to move the cluster from one stable formation to another, and formation keeping, in which the spacecraft remain in a stable formation to within a specified tolerance in the presence of disturbances. Whereas these problems are related and can be addressed by similar methodologies, it is important to explore both in detail to ensure accurate performance of the formation as a whole.

Both problems have been addressed in recent literature. A thorough review of the body of work in which both theoretical and practical solutions and applications for the single-satellite linearized rendezvous problem have been offered is given in Refs. 8 and 9, as well as by Carter.[10] Formation-keeping algorithms have been constructed using several control techniques, including traditional feedback control[11] and higher-order orbit descriptions,[12] but these solutions do not adequately address formation maneuver problems, such as minimizing fuel across a fleet of spacecraft transiting between stable formations about an elliptical orbit.

The formation-keeping problem has also been addressed using convex optimization,[13] which discretizes the trajectory in terms of the true anomaly and integrates constraints such as error boxes and thrust saturation in a parallelizable approach. These techniques were also applied to the formation-maneuvering problem in Ref. 13 a low-eccentricity example of a linear programming solution for generating thrust maps is shown. As described in Ref. 13, however, the computational burden of the linear program increases as the number of discretization points along the trajectory increases. Several methods for resolving this problem are proposed, including coarser discretization, application of constraints at only a subset of points, and the use of a receding horizon (in the formation keeping only), each at the expense of performance (typically fuel usage or final position accuracy). In addition, whereas the linear programs can be shown to be optimal, they are only optimal for the discretized system, not the originating continuous-time system.

For maneuvering, other solutions often rely on finite horizon planning with quadratic cost thrust,[14] consider only impulsive thrusts with quadratic cost,[15] or examine low-Earth orbits.[16] Whereas finite horizon methods are adaptable and effective, they are also computationally intensive when used for clusters and frequently rely on specialty software. Quadratic costs, meanwhile, tend to simplify the problem but do not adequately represent the large class of high specific impulse, low-thrust devices that are the most realistic for use on precision formations of satellites[17,18]; Ross[19] shows that the use of a quadratic cost can require up to 50% more fuel usage when compared to the more appropriate absolute fuel cost. Finally, restrictions to low altitudes limit applicability to high-Earth-orbiting clusters with relatively high eccentricities, such as the magnetospheric multiscale (MMS) mission.[1]

The objective of this work is to construct a full-maneuver planning and control methodology that is optimal across a cluster of spacecraft in formation about a general elliptical orbit, extending the work in Ref. 5. The approach uses a direct point-to-point analysis for the general linearized relative orbit, which is then built into a formation-optimal control methodology. The approach is unique in that it develops formation maneuvers that are provably optimal across the entire cluster, works well in all regimes for which the linearization is valid, considers absolute thrust limitations, and is flexible for solving problems involving any cost using fuel and time. As shown in Ref. 5 and 20, it can also be expanded to work with additional constraints, such as those on collision avoidance, and is computationally tractable and parallelizable across the individual spacecraft in a cluster.

The paper is presented as follows. First, a summary of the relative orbital dynamics is presented as a basis for the formation planning work. Key to this work is the ability to generate point-to-point optimal control solutions for a single spacecraft as quickly as possible. To this end, a spline method is presented that allows the state transition matrix for the relative dynamics to be written analytically and, therefore, used in the development of optimal controllers. The spline work is general enough that it can be applied to a variety of other related problems, such as those that include nonspherical gravitational effects.[21] Next, a thorough treatment of formation parameterizations is given. This is important to the overall methodology because, unique to formation maneuvering, the cluster optimal (fuel or time) plan attempts to minimize the cost across the fleet as a function of these parameters. Finally, the formation optimal control methodology is outlined using the described tools and is applied to an example of a four-spacecraft tetrahedron formation.

Received 22 December 2003; revision received 22 February 2005; accepted for publication 7 March 2005.

*Graduate Student, Aerospace Engineering.

†Professor, Department of Mechanical and Aerospace Engineering. Senior Member AIAA.

II. Relative Orbital Dynamics

The relative dynamics of a spacecraft about an elliptical reference orbit are generally given by a local linearization. A key aspect of the work presented here is defining the state propagation as an analytic function via the state transition matrix. When procedures outlined in Refs. 22–24 are used, the equations of motion for a satellite in a general force field $f(\boldsymbol{R})$ with thrust $\boldsymbol{T}$ are given by

$$\ddot{\boldsymbol{r}} = -f(\boldsymbol{R})\boldsymbol{r} - f'(\boldsymbol{R})[(\boldsymbol{R}\cdot\boldsymbol{r})/|\boldsymbol{R}|]\boldsymbol{R} + \boldsymbol{T}/m \tag{1}$$

where $\boldsymbol{R}_{\text{ref}}$ is the position of a reference satellite with respect to the center of gravitational attraction, $\boldsymbol{r}$ is the relative position of the spacecraft from this reference, and $|\boldsymbol{r}| \ll |\boldsymbol{R}_{\text{ref}}|$.

When transformed to a rotating frame centered on the reference orbit, where the x_3 axis points in the direction of the reference orbit angular momentum vector, x_2 is aligned with the position vector $\boldsymbol{R}$, and x_1 completes the right-hand set, the relative and absolute positions become $\boldsymbol{r} = (x_1, x_2, x_3)$ and $\boldsymbol{R} = (0, R, 0)$, with the rotational velocity of the satellite given by $\Omega = (0, 0, \omega)$.

In a general elliptical orbit, the position and velocity are functions of the true anomaly θ, so that $\boldsymbol{R} = \boldsymbol{R}(\theta)$ and $\omega = \omega(\theta)$. In the following derivation, let $(\cdot)'$ denote differentiation with respect to θ. When Eq. (1) and the conservation of angular momentum $R^2\omega = \text{const} = L$ are used, the relative position and velocity are normalized via

$$y_i = \omega(\theta)^{\frac{1}{2}} x_i, \qquad v_i = y_i', \qquad u_i = T_i/m \tag{2}$$

The generalized force can be rewritten as $G[\omega(\theta)] = -\omega(\theta)^{-2} f'(\boldsymbol{R})\boldsymbol{R}$, and the motion is represented by a linear equation. In the case of a general Newtonian gravitational field,

$$G[\omega(\theta)] = -\frac{\mathrm{d}}{\mathrm{d}R}\left(\frac{\mu}{R(\theta)^3}\right)\frac{R(\theta)}{\omega(\theta)^2} \tag{3}$$

where μ is the constant of gravitational attraction of the central body.

The transformed system has a propagation equation

$$\boldsymbol{z}(\theta) = \Phi(\theta)\Phi^{-1}(\theta_0)\boldsymbol{z}(\theta_0) + \Phi(\theta)\int_{\theta_0}^{\theta} \Phi^{-1}(\tau)B(\tau)\boldsymbol{u}\,\mathrm{d}\tau \tag{4}$$

where $\boldsymbol{z}(\theta) = (y_1, v_1, y_2, v_2, y_3, v_3)$ and $\Phi(\theta)$ and its inverse are as given by Carter,[10] with the correction that

$$\phi_3'(\theta) = 6e\phi_1'(\theta)K(\theta) + \frac{6e\sin^3\theta}{\rho(\theta)^3} - \frac{4\sin\theta(e+\cos\theta)}{\rho(\theta)^3} + \sin\theta\cos\theta\frac{(2+e\cos\theta)}{\rho(\theta)^2} + 2\sin\theta\cos\theta$$

$$K(\theta) = \int \frac{\sin^2\theta}{\rho(\theta)^4}\,\mathrm{d}\theta$$

$$\rho(\theta) = 1 + e\cos\theta$$

as in Appendix A. This solution is valid for eccentricities $0 \le e < 1$.

When

$$\boldsymbol{Q}[\theta_0, \theta] = \int_{\theta_0}^{\theta} \Phi^{-1}(\tau)B(\tau)\boldsymbol{u}\,\mathrm{d}\tau \tag{5}$$

is defined, the state propagation equation is simply

$$\boldsymbol{z}(\theta) = \Phi(\theta)\Phi^{-1}(\theta_0)\boldsymbol{z}(\theta_0) + \Phi(\theta)\boldsymbol{Q}[\theta_0, \theta] \tag{6}$$

This equation captures only linearized motion, though it could be extended to incorporate nonlinear perturbations. When $\boldsymbol{y}(\theta) = (y_1, y_2, y_3)^T$ and $\boldsymbol{v}(\theta) = (v_1, v_2, v_3)^T$, the unnormalized relative states can be recovered using

$$\boldsymbol{x}(\theta) = \left(L^{\frac{3}{2}}/\mu\right)[\boldsymbol{y}(\theta)/\rho(\theta)] \tag{7}$$

$$\dot{\boldsymbol{x}}(\theta) = \left(\mu/L^{\frac{3}{2}}\right)[e\sin\theta\boldsymbol{y}(\theta) + \rho(\theta)\boldsymbol{v}(\theta)] \tag{8}$$

III. Analytical Approximations of State Propagation

A solution to the state propagation [Eq. (6)] is dictated by the solvability of $\boldsymbol{Q}[\theta_0, \theta]$. When the transformations

$$\sin E = \frac{\sqrt{1-e^2}\sin\theta}{\rho(\theta)}, \qquad \cos E = \frac{\cos\theta + e}{\rho(\theta)} \tag{9}$$

and the identity

$$\omega(\theta) = \rho(\theta)^2/C^2, \qquad C = (L^3/\mu^2)^{\frac{1}{2}} \tag{10}$$

are used, the components of $\boldsymbol{Q}$ become

$$Q(1) = C^3\int_{\theta_0}^{\theta}\left[-2\frac{u_1}{\rho(\theta)^3}\left(3e\rho(\theta)^2K(\theta) - \frac{\sin\theta}{\rho(\theta)}\right) - \frac{u_2}{\rho(\theta)^3} \times \left(-6e^2\rho(\theta)\sin\theta K(\theta) + \frac{2e\sin^2\theta}{\rho(\theta)^2} - \frac{\cos\theta}{\rho(\theta)}\right)\right]\mathrm{d}\theta \tag{11}$$

$$Q(2) = \frac{-2u_1C^3}{(1-e^2)^{\frac{5}{2}}}\left[\left(\frac{e^3}{2} - e\right)E + \sin E - \frac{e}{4}(E + \sin E\cos E)\right] - \frac{u_2C^3}{(1-e^2)}\cos E \tag{12}$$

$$Q(3) = \frac{u_1C^3}{(1-e^2)^{\frac{5}{2}}}\left[E - 2e\sin E + \frac{e^2}{2}(E + \sin E\cos E)\right] \tag{13}$$

$$Q(4) = C^3\int_{\theta_0}^{\theta}\left[-\frac{u_1}{\rho(\theta)^3}\left(-6\rho(\theta)^2K(\theta) - \frac{2\sin\theta\cos\theta}{\rho(\theta)} - \sin\theta\cos\theta\right) - \frac{u_2}{\rho(\theta)^3}\left(6e\rho(\theta)\sin\theta K(\theta) - \frac{2\sin^2\theta}{\rho(\theta)^2} - \frac{\cos^2\theta}{\rho(\theta)} - \cos^2\theta\right)\right]\mathrm{d}\theta \tag{14}$$

$$Q(5) = \frac{-u_3C^3}{(1-e^2)^2}\left(\frac{e}{2}\cos^2 E - \cos E\right) \tag{15}$$

$$Q(6) = u_3C^3\left(\frac{\sin\theta}{\rho(\theta)^3} - 3eK(\theta)\right) \tag{16}$$

There are no singularities at $e = 0$ in the closed-form solutions.

A considerable amount of difficulty arises when attempting to evaluate $Q(1)$ and $Q(4)$ because no closed-form solution has been found for the integration of $\rho(\theta)^{-1}K(\theta)$. However, because the planner methodology derived in this work is based on analytical models, a good approximation of the integral is sufficient.

One relatively precise method for approximating integrals is to use a set of piecewise polynomials (PP) to form a spline function. Consider a real, continuous function $g(x)$, with a series of m breakpoints, or knots, defining the endpoints of $m-1$ intervals on that function: $g(t_0), g(t_1), \ldots, g(t_m)$. The PP approximation for each interval is a kth-order polynomial representation identically equal to $g(x)$ at the endpoints of the interval, such that

$$\hat{g}_i(x) = a_0 + a_1x + a_2x^2 + \cdots + a_{k-1}x^{k-1}, \qquad t_{i-1} \le x \le t_i \tag{17}$$

where

$$\hat{g}_i(t_{i-1}) = g(x)\big|_{x=t_{i-1}}, \qquad \hat{g}_i(t_i) = g(x)\big|_{x=t_i} \tag{18}$$

The collection of polynomials is a spline of the function, written compactly as $\hat{g}_{\mathrm{PP}}(x) = [\hat{g}_1(x \in [t_0, t_1]), \hat{g}_2(x \in [t_1, t_2]), \ldots]$; the spline is continuous because $\hat{g}_{\mathrm{PP}}(t_i) = \hat{g}_i(t_i) = \hat{g}_{i+1}(t_i)$. Also, because $\hat{g}_{\mathrm{PP}}(x)$ is a continuous function of polynomials, its integral is continuous and has the same breakpoints as the original spline. The accuracy of the representation of certain functions is particularly sensitive to the order k, the location and number of knots.

In general, note that the error in the integral over any segment in such a spline approximation will never deviate from the true value by more than

$$\max_{x \in [t_{i-1}, t_i]} [\hat{g}_i(x) - g(x)] \times (t_i - t_{i-1})$$

A spline representation is clearly not unique, and an effective method of determining coefficients on each spline segment attempts to minimize the maximum error over each segment. The method employed for this survey is de Boor's algorithm. A complete treatment of the construction of PP interpolants can be found in Refs. 25 and 26.

Consider now each of the integrands of $Q(1)$ and $Q(4)$ from Eqs. (11) and (14) as the originating function $g(x)$ for a spline. These functions are continuous and differentiable, so that an approximation over some arbitrary interval approaches the exact value as knot spacing approaches zero. To illustrate the usefulness of the approximation, consider a spacecraft orbiting Earth at altitude $2Re$ that thrusts radially for a quarter orbit from apogee, then against-track to perigee. The 2-norm of the position error when the spaceraft returns to apogee is calculated as the difference between the position using a numerical solver and the position using a spline approximation of Eqs. (11) and (14). As shown in Fig. 1, this error drops off dramatically using fewer than 20 kn for a fourth-order spline, even as eccentricity increases. To ensure feasibility of results, all examples in this paper utilize 512 kn per orbit. Because this is simply a function call, the large number of knots has minimal effects on the overall computational time.

Propagation of the state of the system can now be performed for any given series of finite width inputs $\boldsymbol{u}^1, \boldsymbol{u}^2, \ldots, \boldsymbol{u}^j$, from which minimum-time and minimum-fuel planners can be derived. The final state of the system is

$$\boldsymbol{z}(\theta_f) = \Phi(\theta_f)\Phi^{-1}(\theta_0)\boldsymbol{z}(\theta_0) + \Phi(\theta_f)(\boldsymbol{Q}_{u^1}[\theta_1, \theta_2] + \boldsymbol{Q}_{u^2}[\theta_2, \theta_3] + \cdots + \boldsymbol{Q}_{u^j}[\theta_j, \theta_{j+1}]) \tag{19}$$

IV. Formation Parameterization

Cluster optimal maneuvers are defined by minimizing a formation-based cost, subject to varying one or more parameters in the system. Therefore, it is vital for formation optimization to use a parametrization scheme that is both easy to implement and adaptable to as many formation mission problems as possible. To facilitate cluster optimal control, definitions for spacecraft formation parameterizations are introduced.

Based on the stable solutions to the unforced dynamics, each spacecraft within a formation of N satellites can be defined using a set of parameters $\boldsymbol{\Delta} = [\boldsymbol{\Delta}_1, \boldsymbol{\Delta}_2, \ldots, \boldsymbol{\Delta}_N]$, which include those parameters necessary to uniquely define the state of each satellite. Specific definitions for these parameters are given in Sec. IV.A. Related to all spacecraft within the formation is a fleetwide set of formation parameters, described using $\boldsymbol{\Upsilon}$. The approach here, as shown in Sec. IV.A, is to define the formation using a desired shape at only one true anomaly θ_C with a center $\boldsymbol{x}_c = (x_1, x_2, x_3)_c$; this shape can be rotated about any axis and translated.

The complete set of elements for a formation is then given by $\boldsymbol{\Lambda} = [\boldsymbol{\Delta}; \boldsymbol{\Upsilon}, \theta_C]$, and optimization occurs over any subset of elements contained in $\boldsymbol{\Delta}$ (specific to one satellite) or $\boldsymbol{\Upsilon}$ (common to all formation elements). The formation optimal maneuver can then be written compactly as

$$\boldsymbol{\Lambda}_F^* = \min_{\boldsymbol{\Lambda}_F} J_{\mathrm{formation}}(\boldsymbol{\Lambda}_0, \boldsymbol{\Lambda}_F) \tag{20}$$

where $J_{\mathrm{formation}}$ is the formation-based cost, typically a function of time and fuel. Here, $\boldsymbol{\Lambda}_0$ is assumed to be a known initial formation parameter set, whereas some subset of parameters in $\boldsymbol{\Lambda}_F$ is to be optimized over. Note that other variations of the problem are also possible, such as free parameters in $\boldsymbol{\Lambda}_0$, though these problems are generally not useful for onboard applications.

A. Single-Spacecraft Parameterizations, $\boldsymbol{\Delta}_i$

The solution to the cluster-optimal control problem is rooted in the parameterization of the initial state of each member, $\boldsymbol{\Delta}_i$. A stable, unforced initialization for a satellite at an arbitrary point (x_1, x_2, x_3) in the reference frame about the eccentric trajectory at true anomaly θ can be found using the representation given by Inalhan et al.[22] in terms of the original coordinate states x_i. These states can be written in a slightly different and more insightful way as

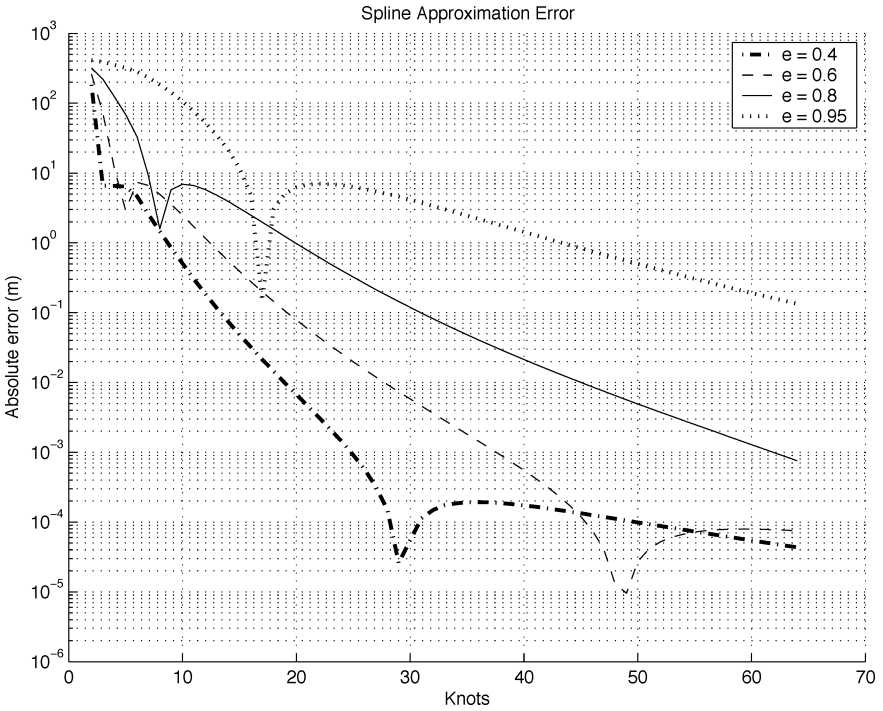

Fig. 1 Fourth-order spline precision as function of knot spacing for various eccentricities; input thrust $u = -6 \times 10^{-5}$ and final position approximately 2.0×10^3 m from reference center.

$$x_1(\theta) = \frac{p_1}{\rho(\theta)} + \left(\frac{1}{\rho(\theta)} + 1\right)(ep_2\cos\theta + p_3\sin\theta) + p_4[2eJ(\theta)\rho(\theta)] \tag{21}$$

$$x_2(\theta) = p_3\cos\theta - ep_2\sin\theta - p_4\left[\frac{e\cos\theta}{\rho(\theta)^2} - 2e^2J(\theta)\right] \tag{22}$$

$$x_3(\theta) = p_5\frac{\sin\theta}{\rho(\theta)} + p_6\frac{\cos\theta}{\rho(\theta)} \tag{23}$$

where

$$J(\theta) = \sin\theta/\rho(\theta) - 3eK(\theta) \tag{24}$$

Note that $J(\theta)$ is not a periodic function. The constants can be arbitrarily chosen to produce an orbit about an elliptical reference, but stable formations, that is, those in which the state repeats after N full orbits, require that the nonperiodic $J(\theta)$ elements be eliminated. Thus, the constant p_4 must be set to 0, and all elements in brackets in Eqs. (21–23) drop out. This leaves five variables to describe all stable relative orbits. From these, the first single-spacecraft parameter set is given as $\boldsymbol{\Delta}_i = [p_1, p_2, p_3, p_5, p_6]$.

The role of each of the constants p_i is readily apparent. In particular, the elements (p_2, p_3) define a circle of radius $\sqrt{[p_3^2 + (ep_1)^2]}$, whereas p_1 defines variable against-track offset at each angle, bounded by $[p_1/(1+e), p_1/(1-e)]$. Figure 2 shows the planar motion of three stable initializations as a function of parameter p_1. Note that these stable orbits are in general not symmetric, experiencing deformations based on the chosen parameter values. The amplitude of the cross-track oscillation is given by $\sqrt{(p_5^2 + p_6^2)}$, and the motion is skewed due to the $\rho(\theta)^{-1}$ relationship.

The corresponding converted z-coordinate position and velocity components can be calculated directly from Eqs. (21–23) using the transformations from Eqs. (7) and (8). The six unforced initialization states become

$$y_1(\theta) = C^{-1}p_1 + C^{-1}[\rho(\theta) + 1](ep_2\cos\theta + p_3\sin\theta) \tag{25}$$

$$v_1(\theta) = [1 + 1/\rho(\theta)]y_2(\theta) - C^{-1}(e\sin\theta)(ep_2\cos\theta + p_3\sin\theta) \tag{26}$$

$$y_2(\theta) = \omega(\theta)^{\frac{1}{2}}(p_3\cos\theta - ep_2\sin\theta) \tag{27}$$

$$v_2(\theta) = -[e\sin\theta/\rho(\theta)]y_2(\theta) - \omega(\theta)^{\frac{1}{2}}(ep_2\cos\theta + p_3\sin\theta) \tag{28}$$

$$y_3(\theta) = C^{-1}(p_5\sin\theta + p_6\cos\theta) \tag{29}$$

$$v_3(\theta) = C^{-1}(p_5\cos\theta - p_6\sin\theta) \tag{30}$$

with $\omega(\theta)$ and C as defined in Eq. (10). Notice that the relationship between y_2 and v_1 approaches that given by Tillerson et al.[13] for initialization at perigee ($\theta = 0$).

The set $\boldsymbol{\Delta}_i$ gives the parameterization for the stable initialization for the ith satellite. This set is clearly not unique because other transformations of the state parameters also provide a parameterization for each cluster member.

B. Centered Parameterizations for Single Spacecraft

For clusters, a reduction of the size of the parameter set of each formation member often provides a more functional means of solving the optimal control problem. Centered formations, or those where $p_1 = 0$ (Fig. 2), are considered in the remainder of this paper. A more detailed analysis of noncentered orbits is given in Ref. 27. Centered formations always encircle the point $(x_1, x_2) = (0, 0)$; the parameter set for a centered orbit can then be written $\boldsymbol{\Delta}^c = \{\boldsymbol{\Delta} | p_1 = 0\}$. For this case, another insightful parameter set can be defined[27] as $\boldsymbol{\Delta}^c_{R,i} = [R, \alpha, R_{x_3}, \alpha_{x_3}]$, where size and phasing parameters are used; under this parameter set, the unforced equations reduce to those given by Campbell[20] for the circular reference orbit.

In the formation optimal planner examined in this paper, the satellite parameterization is defined using a formation shape at the critical true anomaly θ_C. This shape is given by a position basis $\boldsymbol{P}_i$ for each satellite, which locates each member of the formation about the cluster center. The position of the ith spacecraft with respect to this center at θ_C is then given by

$$\boldsymbol{x}_{\Delta_i}(\theta_C) = l \cdot \boldsymbol{P}_i \tag{31}$$

where l is a scaling length and the elements of $\boldsymbol{x}_{\Delta_i}$ correspond to the position elements in Eqs. (21–23). As a simplification, it is assumed that the formation is centered ($p_1 = 0$) and that $\dot{x}_{3,i}(\theta_C) = 0$. This parameterization is given by $\boldsymbol{\Delta}^c_{P,i} = [l\cdot\boldsymbol{P}_i, p_1 = 0, \dot{x}_{3,i}(\theta_C) = 0]$.

As an example, consider four spacecraft arranged in a regular tetrahedron. This formation corresponds to the demands of the MMS mission. It is characterized by position bases that place four satellites unit distance apart:

$$\boldsymbol{P}_{\mathrm{MMS},1} = \begin{pmatrix} 0 \\ \sqrt{3}/2\sqrt{2} \\ 0 \end{pmatrix}, \qquad \boldsymbol{P}_{\mathrm{MMS},2} = \begin{pmatrix} 0 \\ -\sqrt{3}/6\sqrt{2} \\ -\sqrt{3}/3 \end{pmatrix}$$

$$\boldsymbol{P}_{\mathrm{MMS},3} = \begin{pmatrix} -1/2 \\ -\sqrt{3}/6\sqrt{2} \\ \sqrt{3}/6 \end{pmatrix}, \qquad \boldsymbol{P}_{\mathrm{MMS},4} = \begin{pmatrix} 1/2 \\ -\sqrt{3}/6\sqrt{2} \\ \sqrt{3}/6 \end{pmatrix}$$

and is then denoted by the parameterization $\boldsymbol{\Delta}^c_{P_{\mathrm{MMS}}} = \{\boldsymbol{\Delta}^c_P | \boldsymbol{P} = \boldsymbol{P}_{\mathrm{MMS}}\}$.

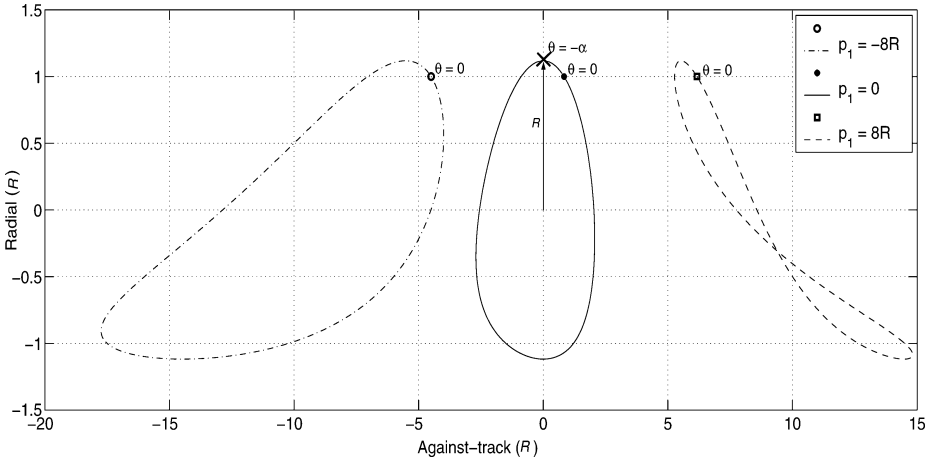

Fig. 2 Effects of the choice of parameter value p_1 at $e = 0.5$: orbits produced by varying p_1 at nonzero eccentricities are both offset and skewed.

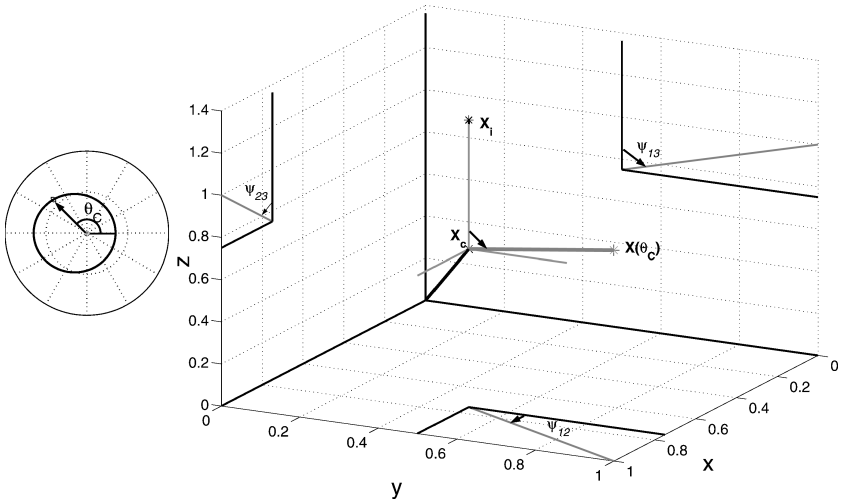

Fig. 3 Position of single spacecraft in relation to formation parameters θ_C, $\boldsymbol{x}_c$, and $(\psi_{12}, \psi_{13}, \psi_{23})$.

C. Formation Parameterizations, $\boldsymbol{\Upsilon}$

A formation of N satellites begins with the definition of a parameter set $\boldsymbol{\Delta}_i$ for each spacecraft. The formation is defined about a centerpoint $\boldsymbol{x}_c$, which can be rotated via Euler rotations T_{ij} about the relative motion coordinate axes through angles $(\psi_{12}, \psi_{13}, \psi_{23})$. As well, the center can be translated to some point $\boldsymbol{x}_c$. The set of rotations, the specification of the formation center, and the number of satellites are invariant over all spacecraft in the formation; such parameters are contained in the formation parameterization set $\boldsymbol{\Upsilon} = [N, \boldsymbol{x}_c, (\psi_{12}, \psi_{13}, \psi_{23})]$. The relationship between the actual position of the satellite at the formation true anomaly θ_C and the elements of the sets $\boldsymbol{\Delta}_i$ and $\boldsymbol{\Upsilon}$ is shown in Fig. 3 and given mathematically by

$$\boldsymbol{x}_i(\theta_C) = \boldsymbol{x}_c + T_{12}T_{13}T_{23}\boldsymbol{x}_{\Delta_i}(\theta_C) \tag{32}$$

Whereas it is possible to define the formation at only true anomaly θ_C, it is important for optimal control purposes to be able to place the spacecraft uniquely on a stable orbit at an arbitrary true anomaly θ using a given parameterization. This can be accomplished by first converting to the $\boldsymbol{z}$ frame via Eqs. (7) and (8), propagating the system through a zero-thrust maneuver to the desired true anomaly, and transforming back to $\boldsymbol{x}$ coordinates. Likewise, the values of p_i can be determined using Eqs. (7), (8) and (25–30),

$$\boldsymbol{x}_i(\theta_C) \xrightarrow{\text{Eqs. (7) and (8)}} \boldsymbol{z}_i(\theta_C) \xrightarrow{\text{Eq. (4)},u=0}$$

$$\boldsymbol{z}_i(\theta) \xrightarrow{\text{Eqs. (7) and (8)}} \boldsymbol{x}_i(\theta) \xrightarrow{\text{Eqs. (7), (8), and (25–30)}} [p_1, \ldots, p_6] \tag{33}$$

The formation can, therefore, be described compactly as $\boldsymbol{\Lambda} = [\boldsymbol{\Delta}; \boldsymbol{\Upsilon}, \theta_C]$. For most optimization problems, the cost is evaluated by varying a subset of the single-spacecraft parameters in $\boldsymbol{\Delta}_i$ and/or the parameters of the formation set $\boldsymbol{\Upsilon}$. To differentiate the optimization variables, the parameter sets can be partitioned into free and fixed parameters such that $\boldsymbol{\Delta}_i = [\boldsymbol{\Delta}_i(\text{free})|\boldsymbol{\Delta}_i(\text{fixed})]$ and $\boldsymbol{\Upsilon} = [\boldsymbol{\Upsilon}(\text{free})|\boldsymbol{\Upsilon}(\text{fixed})]$.

V. Formation Optimal Maneuvers

Time-optimal and fuel-optimal maneuvers for a spacecraft have been widely explored in the last two decades. Most recently, Campbell[5] used relative dynamics and a circular reference orbit to develop formation optimal minimum-time and minimum-fuel planners for satellite formations based on optimal thrust for two inputs. This work extends the approach to the eccentric orbit case using the state propagation equation, the spline approximation in Sec. III, and the formation parameterizations in Sec. IV. Whereas only cluster fuel- and time-optimal formulations are considered here, the results are general and can be integrated into the planning methodology described in Ref. 5, with constraints such as collision avoidance and communication; other considerations may be required as well, depending on the mission demands. As in the circular case, though, solution times must remain under one orbit to guarantee validity.[5]

The formation optimal maneuver between initial cluster parameterization $\boldsymbol{\Lambda}_0$ and final cluster parameterization $\boldsymbol{\Lambda}_F$ is defined by the formation cost,

$$\boldsymbol{\Lambda}_F^* = \min_{\Lambda_F} J_{\text{formation}}(\boldsymbol{\Lambda}_0, \boldsymbol{\Lambda}_F) \tag{34}$$

Formation optimal maneuvers are developed here using single-spacecraft optimal control. The generation of single-spacecraft optimal maneuvers is presented for both minimum-time and minimum-fuel cases. The solution approach is integrated into a methodology to solve Eq. (34).

A. Single-Spacecraft Minimum Time

The cost function for a minimum-time optimal maneuver for a single spacecraft uses the fact that the true anomaly θ increases monotonically with time and can be defined as

$$J_T = \int_{\theta_0}^{\theta_F} \mathrm{d}\theta \tag{35}$$

Because the cross-axis y_3 element is decoupled, the six states in the original optimal control problem are separated into a four-state problem in the orbital plane and a two-state problem out of the orbital plane.

For the in-plane problem and assuming thrust-limited propulsion as with electric thrusters, following Ref. 5, the shape of the time-optimal input for a single spacecraft in the orbital plane is assumed to be a three-switch bang–bang thrust sequence terminating at the minimum time. When the subscript i notation for this section is dropped and the model further simplified to consider thrust input in the along-track direction only, the planar state is $\boldsymbol{z}_p = (y_1, v_1, y_2, v_2)^T$ with state matrices $[A(\theta), B(\theta)]$ defined as

$$A(\theta) = \begin{bmatrix} 0 & 1 & 0 & 0 \\ 0 & 0 & 0 & 2 \\ 0 & 0 & 0 & 1 \\ 0 & -2 & G[\omega(\theta)] & 0 \end{bmatrix}, \qquad B(\theta) = \begin{pmatrix} 0 \\ \omega(\theta)^{-\frac{3}{2}} \\ 0 \\ 0 \end{pmatrix} \tag{36}$$

The initial condition $\boldsymbol{z}_p(\theta_0)$ is assumed to be known. Let $\boldsymbol{Q}^p$ be the first four elements of the $\boldsymbol{Q}$ vector, given in Eqs. (11–14). The

elements of the jth input vector $\boldsymbol{Q}_j^p$ on each of the four constant-thrust intervals $[\theta_{j-1}, \theta_j]$ become

$$\boldsymbol{Q}_j^p[\theta_{j-1}, \theta_j] = (-1)^{j-1} u \begin{pmatrix} -2S\left[S[\phi_2(\theta)]\omega(\theta)^{-\frac{3}{2}}\right] \\ 2S\left[S[\phi_1(\theta)]\omega(\theta)^{-\frac{3}{2}}\right] \\ S\left[\omega(\theta)^{-\frac{3}{2}}\right] \\ -S\left[S[\phi_3(\theta)]\omega(\theta)^{-\frac{3}{2}}\right] \end{pmatrix}\Bigg|_{\theta_{j-1}}^{\theta_j}$$

Note that spline construction can be performed a priori using only the orbital data. Thus, the computation time does not generally increase as the number of knots increases.

From the adjoint system,

$$\boldsymbol{\lambda}'(\theta) = -A^T(\theta)\boldsymbol{\lambda}(\theta) \tag{37}$$

the Hamiltonian can be defined as

$$\mathcal{H}_T(\theta) = 1 + \boldsymbol{\lambda}^T(\theta)\left[A(\theta)\boldsymbol{z}_p(\theta) + B(\theta)(-1)^{j-1}u\right] \qquad \theta_{j-1} \le \theta \le \theta_j \tag{38}$$

The costate at any true anomaly θ is

$$\boldsymbol{\lambda}(\theta) = \Psi_{[1-4]}(\theta)\Psi_{[1-4]}^{-1}(\theta_0)\boldsymbol{\lambda}_0 \tag{39}$$

where the full matrix Ψ is given by Carter[10] and shown in Appendix B. The notation $[\cdot]_{[r-s]}$ represents the $(s-r+1)\times(s-r+1)$ square partition of the referenced matrix $[\cdot]$ containing both $[\cdot](r, r)$ and $[\cdot](s, s)$.

The constraints to be satisfied for the time-optimal control problem for a single spacecraft are

$$\boldsymbol{z}_p\left(\theta_F^*\right) = \Phi_{[1-4]}\left(\theta_F^*\right)\Phi_{[1-4]}^{-1}(\theta_0)\boldsymbol{z}_p(\theta_0) + \Phi_{[1-4]}\left(\theta_F^*\right)\left(\boldsymbol{Q}_1^p\left[\theta_0, \theta_1^*\right] + \boldsymbol{Q}_2^p\left[\theta_1^*, \theta_2^*\right] + \boldsymbol{Q}_3^p\left[\theta_2^*, \theta_3^*\right] + \boldsymbol{Q}_4^p\left[\theta_3^*, \theta_F^*\right]\right) \tag{40}$$

$$\boldsymbol{\lambda}^T\left(\theta_i^*\right)B\left(\theta_i^*\right) = 0, \qquad i = 1, 2, 3 \tag{41}$$

$$\mathcal{H}_T\left(\theta_F^*\right) = 0 \tag{42}$$

with $\boldsymbol{z}_p(\theta_F)$ determined as described in Eq. (33). Values θ_i^* represent the true anomaly values at which the control input switches. This problem has eight unknowns: three switches $(\theta_1^*, \theta_2^*, \theta_3^*)$, the final time for the maneuver (θ_F^*), and four initial conditions on the costate $(\boldsymbol{\lambda}_0)$. There are also eight constraint equations; note that all switch times θ_i^* are solvable independent of the costate. Thus, the costate solution simply verifies optimality. When the final angle θ_F is used as a free parameter representing the shutoff time for the thrust inputs, the constraint equations for the input times can be solved numerically.

The cross-axis problem consists of a two-state system that is decoupled from the in-plane problem. The minimum-time control input for maneuvering under one orbit is again bang–bang, consisting of a single switch (θ_1^*) and a shutoff time (θ_F^*). The dynamics in the rotating z frame are given by

$$\begin{pmatrix} y_3 \\ v_3 \end{pmatrix}' = \begin{bmatrix} 0 & 1 \\ -1 & 0 \end{bmatrix}\begin{pmatrix} y_3 \\ v_3 \end{pmatrix} + \begin{bmatrix} 0 \\ \omega(\theta)^{-\frac{3}{2}} \end{bmatrix} u_3 \tag{43}$$

Let $\boldsymbol{Q}_i^{z_3}$ be the two-element vector $[Q_i(5), Q_i(6)]^T$, and recall from Eqs. (15) and (16) that this input vector has a closed-form solution. When $\boldsymbol{z}_3 = (y_3, v_3)^T$ and the out-of-plane costate similar to the planar costate are defined as $\boldsymbol{\lambda}_{z_3}(\theta)$, the optimal thrust constraints are

$$\boldsymbol{z}_3\left(\theta_F^*\right) = \Phi_{[5-6]}\left(\theta_F^*\right)\Phi_{[5-6]}^{-1}(\theta_0)\boldsymbol{z}_3(\theta_0) + \Phi_{[5-6]}\left(\theta_F^*\right)\left(\boldsymbol{Q}_1^{z_3}\left[\theta_0, \theta_1^*\right] + \boldsymbol{Q}_2^{z_3}\left[\theta_1^*, \theta_F^*\right]\right) \tag{44}$$

$$\boldsymbol{\lambda}_{z_3}^T\left(\theta_i^*\right)B_{z_3}\left(\theta_i^*\right) = 0, \qquad i = 1, 2, 3 \tag{45}$$

$$\mathcal{H}_{z_3,T}\left(\theta_F^*\right) = 0 \tag{46}$$

B. Single-Spacecraft Minimum Fuel

The single-spacecraft minimum-fuel problem uses a cost function defined as

$$J_F = \int_{t_0}^{t_F} \|\boldsymbol{u}\|\,\mathrm{d}t \tag{47}$$

with $\|\cdot\|$ denoting the 2-norm of the vector. The time dependence of this cost must first be converted to true anomaly to solve using the true anomaly-based dynamics used here. The time and true anomaly differentials are related by

$$\mathrm{d}t = \sqrt{a^3/\mu}\left[(1-e^2)^{\frac{3}{2}}/\rho(\theta)^2\right]\mathrm{d}\theta = \omega(\theta)^{-1}\,\mathrm{d}\theta \tag{48}$$

The solution is assumed to be bang–off-bang, with the planar maneuver beginning at time θ_0 and ending at time θ_F. The planar solution consists of four thrust segments and is defined by six unknowns. In this case, the constraints for the minimum-fuel problem are given by

$$\boldsymbol{z}_p(\theta_F) = \Phi_{[1-4]}(\theta_F)\Phi_{[1-4]}^{-1}(\theta_0)\boldsymbol{z}_p(\theta_0) + \Phi_{[1-4]}(\theta_F)\left(\boldsymbol{Q}_1^p\left[\theta_0, \theta_1^*\right] + \boldsymbol{Q}_2^p\left[\theta_1^*, \theta_2^*\right] + \boldsymbol{Q}_3^p\left[\theta_2^*, \theta_3^*\right] + \boldsymbol{Q}_4^p\left[\theta_3^*, \theta_F\right]\right) \tag{49}$$

$$\boldsymbol{\lambda}^T\left(\theta_i^*\right)B\left(\theta_i^*\right) = -\mathrm{sgn}\left[u\left(\theta_i^*\right)\right]\omega(\theta)^{-1}, \qquad i = 1, 2, 3, 4, 5, 6 \tag{50}$$

where $\mathrm{sgn}(u)$ indicates

$$\begin{aligned} u(\theta) = u, \quad &\text{for} \quad \boldsymbol{\lambda}^T(\theta)B(\theta) < -\omega(\theta)^{-1} \\ u(\theta) = 0, \quad &\text{for} \quad -\omega(\theta)^{-1} \le \boldsymbol{\lambda}^T(\theta)B(\theta) \le +\omega(\theta)^{-1} \\ u(\theta) = -u, \quad &\text{for} \quad \boldsymbol{\lambda}^T(\theta)B(\theta) > +\omega(\theta)^{-1} \end{aligned} \tag{51}$$

and $\boldsymbol{\lambda}(\theta)$ is given by Eq. (39). Unlike the minimum-time problem, the solution for the switching true anomalies is coupled with the costate, resulting in 10 coupled nonlinear equations. These equations can be reduced to 6 coupled nonlinear equations by first finding $\boldsymbol{\lambda}_0$ through the overdetermined matrix costate equation

$$\begin{bmatrix} B(\theta_1)^T\Psi(\theta_1) \\ \hline B(\theta_2)^T\Psi(\theta_2) \\ \hline \vdots \\ \hline B(\theta_6)^T\Psi(\theta_6) \end{bmatrix}\Psi(\theta_0)^{-1}\boldsymbol{\lambda}_0 = \begin{bmatrix} \omega(\theta_1)^{-1} \\ \hline \omega(\theta_2)^{-1} \\ \hline \vdots \\ \hline \omega(\theta_6)^{-1} \end{bmatrix} \tag{52}$$

The cross-axis maneuver is assumed to occur during the same time period $[\theta_0, \theta_F]$, but to allow more solution flexibility, it is not assumed to begin and end at these points. Instead, it is a two-thrust sequence with four unknown switches and two initial costate elements. The solution is found by the equations

$$\boldsymbol{z}_3(\theta_F) = \Phi_{[5-6]}(\theta_F)\Phi_{[5-6]}^{-1}(\theta_0)\boldsymbol{z}_3(\theta_0) + \Phi_{[5-6]}(\theta_F)\left(\boldsymbol{Q}_1^{z_3}\left[\theta_1^*, \theta_2^*\right] + \boldsymbol{Q}_2^{z_3}\left[\theta_3^*, \theta_4^*\right]\right) \tag{53}$$

$$\boldsymbol{\lambda}_{z_3}^T\left(\theta_i^*\right)B_{z_3}\left(\theta_i^*\right) = -\mathrm{sgn}\left(u\left(\theta_i^*\right)\right)\omega(\theta)^{-1}, \qquad i = 1, 2, 3, 4 \tag{54}$$

which can be reduced to four equations in a manner similar to the planar case.

VI. Simulation Results

To examine formation optimal planners, consider a tetrahedral formation of four satellites, as described in Sec. IV.c. The orbital data and formation correspond to the proposed MMS mission,[1] a cluster that will operate in medium- to high-altitude orbits with $e \gtrsim 0.7$. The scientific goals of MMS require the formation to be a tetrahedron with leg length approximately 1 km at apogee, with no constraints on formation orientation; the tetrahedron can reconfigure its size and

orientation during each orbit. The objective of the formation planner is to optimize such a reconfiguration to leg length 1.1 km starting at apogee and finishing before the following apogee over the final Euler angle $\psi_{12,F}$ based on the formation cost. For this problem, both formation optimal minimum-time and minimum-fuel solutions are generated. (See Table 1.) Although motion occurs in three dimensions, the cross-axis is invariant under rotations about ψ_{12} and, therefore, does not enter the formation optimization problem.

A. Minimum Time

The formation minimum-time control problem is defined as

$$\boldsymbol{\Lambda}_F^* = \min_{\psi_{12}} \max_{i\in[1,\ldots,4]} J_{T,i} \tag{55}$$

The minimum maneuver time and the optimal final cluster rotation angle ψ_{12} can be found using Fig. 4, which gives the single-spacecraft minimum-time solutions at each angle. The cluster minimum solution, which corresponds to the worst-case single-satellite minimum time, is shown in bold. The four-satellite optimal plan results in the smallest cluster minimum time, which occurs at approximately $\psi_{12,F} = 2.3$ deg; at this point, the cluster maneuver time is 7% less than with zero rotation ($\psi_{12} = 0$ deg). This shows that, although the final rotation is small, significant cost savings can be attained by considering a cluster optimal solution.

In this problem, 63 evaluations of $\psi_{12,F}$ were made for each spacecraft by performing two scans. First, the profile of $\psi_{12,F} \in [-90, 90]$ deg was scanned using 33 evenly spaced points. Then the central region of $\psi_{12,F} \in [-5.625, 5.625]$ deg, where the coarse profile shows a minimum, was further scanned using a fine grid of 32 points with 0.35-deg spacing. The fine-grid scan, which requires only a good initial profile and can, therefore, be initialized using partial a priori solution information, requires less than 5 s to evaluate each point using a MATLAB® implementation on a Pentium IV, 1.8-GHz machine. Because the process is parallelizable, each spacecraft can evaluate its own profile, and the planner implementation in this region can be performed in ~3 min. Clearly, a C/C++ implementation and a more effective scanning routine would further speed this solution process.

Table 1 Initial and final parameter values for example simulation

	Parameter	Initial	Final
Reference	a	12 Re	12 Re
	e	0.8	0.8
	μ	3.986012×10^5	3.986012×10^5
$\boldsymbol{\Lambda}_i$ θ_C		π	π
$\boldsymbol{\Lambda}_i$ $\boldsymbol{\Delta}_i$	$l \cdot \boldsymbol{P}_i$	1.0 km $\cdot \boldsymbol{P}_i$	1.1 km $\cdot \boldsymbol{P}_i$
	p_1	0	0
	$\dot{x}_3(\theta_C)$	0	0
$\boldsymbol{\Lambda}_i$ $\boldsymbol{\Upsilon}$	N	4	4
	$\boldsymbol{x}_c$	(0, 0, 0)	(0, 0, 0)
	$(\psi_{12}, \psi_{13}, \psi_{23})$	(0, 45, 45) deg	(ψ_{12}, 45, 45) deg

The three-dimensional motion of this cluster-optimal maneuver is shown in Fig. 5. It is evident that the spacecraft both begin and end in a tetrahedron formation, although they are not in this formation at intermediate points. The maneuver is completed at a true anomaly of $\theta_F = 5.25$ rad, or before the four satellites reach perigee. Therefore, the second-half of the trajectory occurs under unforced, stable dynamics. Note that collision avoidance is not considered here and is unnecessary for this example due to the large spacing beteen the spacecraft, but it could in general be added as a constraint as in Ref. 20.

B. Minimum Fuel

A formation-optimal minimum-fuel plan is generated using the sum of the fuel usage over all spacecraft. This is given as

$$\boldsymbol{\Lambda}_F^* = \min_{\psi_{12}} \sum_{i=1}^{4} J_{F,i} \tag{56}$$

for a fixed final true anomaly θ_F. From Eqs. (47) and (48), it is clear that the cost for large eccentricities is weighted toward thrusts occurring near perigee, where a small input is most effective at changing the trajectory of the satellite. With this objective, the fuel-optimal cost for each satellite and the fleetwide minimum-fuel solutions for the sample problem are shown in Fig. 6 for a final true anomaly of 0.92 orbits past apogee, such that $\theta_F = \theta_0 + 0.92(2\pi)$. Figure 6 has been truncated to show the region of importance; cost increases significantly outside the region shown. The cluster minimum occurs at zero rotation ($\psi_{12} = 0$ deg), where a savings of 94% in fuel use is attained over the minimum-time solution.

The planar single-spacecraft minimum-fuel solution can have up to six switches and as few as four switches, depending on the final true anomaly. Figure 7 shows the switch times and fuel as a function of the end maneuver time θ_F. For small θ_F, the solution includes six switches and follows a profile that closely resembles the minimum-time solution with brief intermediate coasts. For small increases in θ_F, however, the fuel cost quickly decreases, indicating that a smart planning methodology can save significant amounts of fuel without requiring a significant time expenditure. As θ_F increases, the thrust traverses a variety of thrust profiles, and the fuel cost is nonincreasing with θ_F. In addition, there is continuity between segments in which the thrust profile changes.

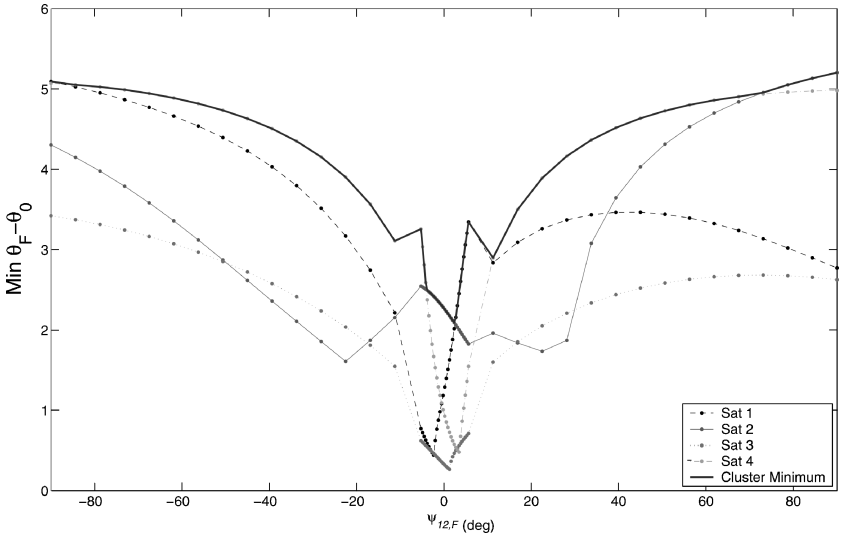

Fig. 4 Minimum-time solution for variable ψ_{12} for example problem: ——, cluster minimum time at each angle, with optimal final angle $\psi_{12} = 2.3$ deg.

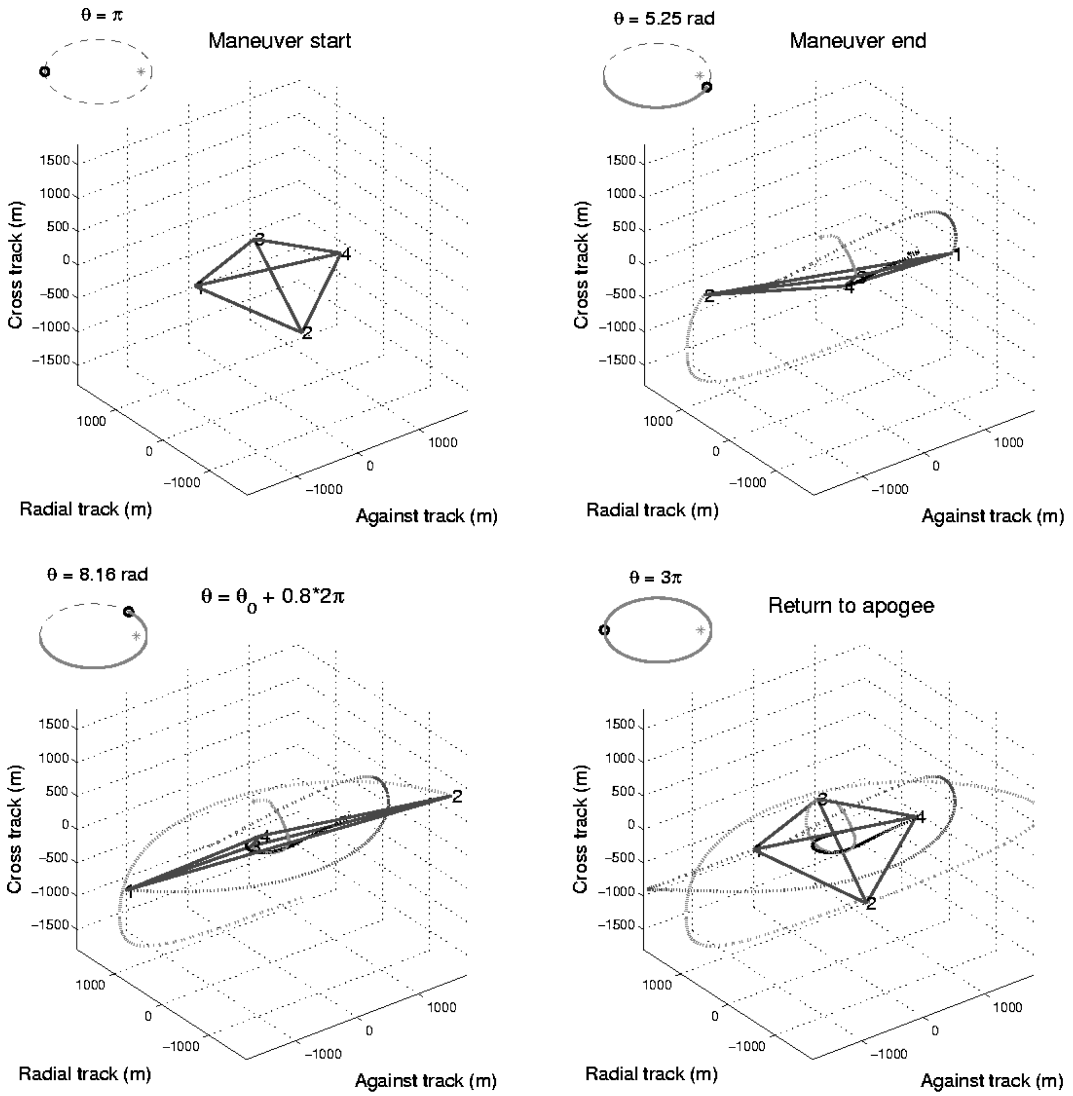

Fig. 5 Trajectory of a tetrahedral satellite formation change at apogee for eccentricity $e = 0.8$ and reference altitude 12 *Re*: formation begins in regular tetrahedron of leg length 1.0 km (top left), proceeds through its series of thrusts (top right), coasts back to apogee (lower left and right), and ends as a regular tetrahedron of leg length 1.1 km.

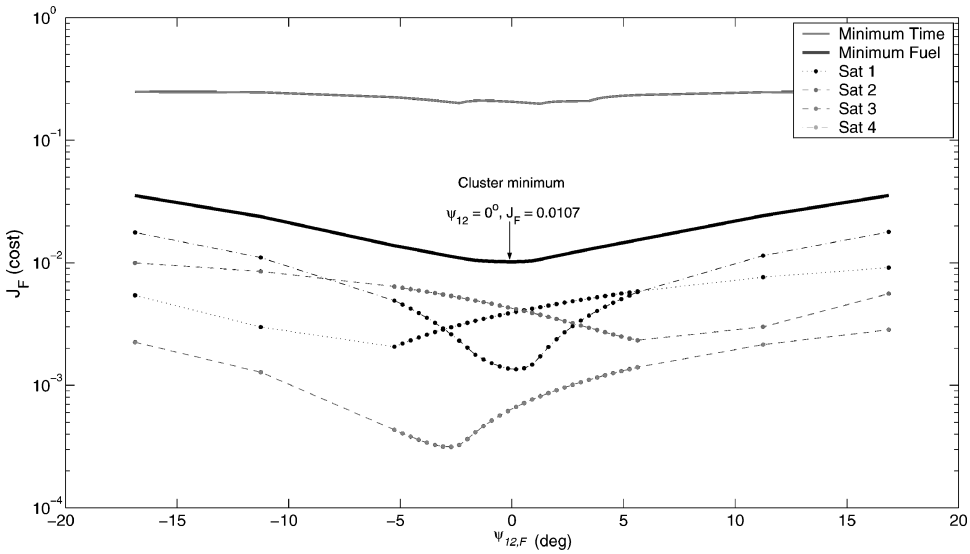

Fig. 6 Minimum-fuel solution with final maneuver true anomaly of $\theta_F = \theta_0 + 0.92$ orbits for varying final angle ψ_{12} for the example problem: ——, total cost for all four satellites at each angle, with optimal $\psi_{12,F} = 0$ deg.

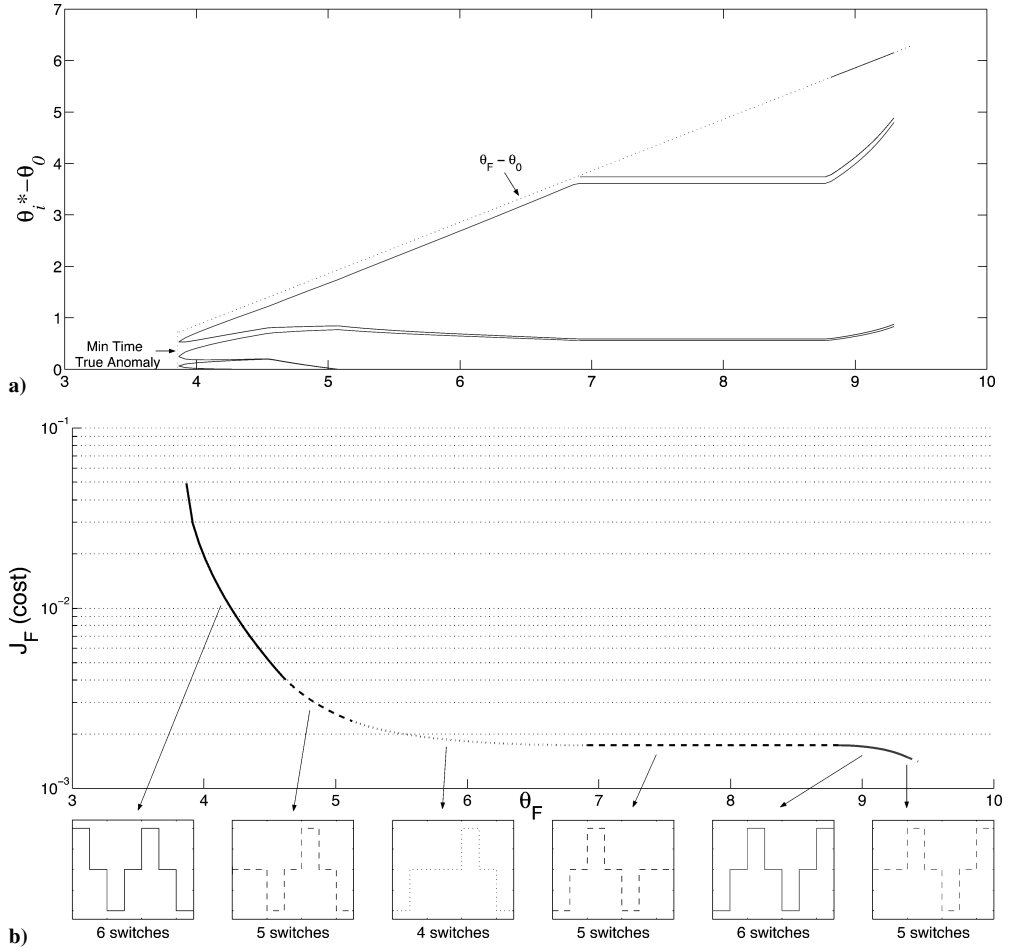

Fig. 7 Minimum-fuel solution varies with θ_F: a) individual switches for fourth satellite at offset of 1.27 deg and b) total fuel cost and corresponding switch profiles.

Calculation time for this problem is again dependent on the number of samples. The region shown contains 34 points and was generated using a coarse grid of 7 points evenly spaced across the range $\psi_{12} \in [-17, 17]$ deg and a fine mesh of 30 constantly spaced points for the inner region of $\psi_{12} \in [-5.625, 5.625]$. The initialization strategy employed here considers small variations in the final true anomaly, starting with the minimum-time true anomaly; each point on the fine grid requires less than 30 s per satellite to solve in MATLAB on a Pentium IV, 1.8-GHz computer. Run in parallel, the formation planner needs ~15 min to complete the optimization. In general, this computation time can be reduced through a more efficient initialization scheme and the use of C/C++ programming. For instance, once one point on the fuel curves is found, all subsequent points can be found by using the previous solution as an initial guess. This approach has worked well in practice in reduning computation time to several seconds per point per satellite.

Also note that the solution time is invariant with the number of spline segments. When repeating the preceding example for cases ranging from 20 to 512 kn, no measurable increase in computation time was found.

C. Comparison with Linear Programming

The method examined in the previous example is provably optimal for the time-varying, linearized state propagation form given in Eq. (6) and is, therefore, able to outperform any technique relying on discretization in the linear regime. In this section, the performance of the Hamilton–Jacobi–Bellman (HJB) optimization method is compared to linear programming (LP), which has been shown to generate near-optimal solutions quickly for some eccentric orbit problems.[13]

The problem shown in Fig. 7 was solved using an LP in MATLAB. The LP was posed by discretizing the orbit into 1000 points. Identical constraints on thrust (6×10^{-5} N) and final relative position and velocity (10 m, 2 m/s) were used for both solution approaches. Note that a final position constraint is used in the HJB solution by selecting the tolerance on the constraint equations (40), (44), (49), and (53).

Simulation results show a 15% fuel savings of the HJB approach compared to that of the linear program. The computational solution times were comparable (several seconds per solution) in both cases. Increasing the number of discretization points to 10,000 points decreases the fuel savings to 10%, indicating that the LP solution is a function of the discretization. This is most evident when the eccentricity is large ($e = 0.8$) and the system matrices are time varying. Computational time in this case increases to tens of seconds for the LP solutions. When the eccentricity for this example is decreased to $e = 0.005$ (the same used in Ref. 13), the LP solutions are 1.5% higher on average than the HJB solutions, indicating that sensitivity to eccentricity is a factor in the LP solutions. Finally, when the constraint on the final position and velocity is increased by a factor of 10 for the $e = 0.8$ case, the average savings in fuel usage for the HJB solutions is 5.4%. If the constraint on the final position and velocity is decreased by a factor of 10, the average fuel savings for the HJB solutions is 33%. In all cases, the LP solutions show chatter about the expected switch times, and this chatter increases as higher accuracy in the endpoint is required. This indicates that the LP solution uses additional thrust (and increasing fuel usage) in an attempt to overcome discretization errors and attain final endpoint accuracy.

VII. Conclusions

A methodology has been described for constructing formation optimal maneuvers for satellites with bounded thrust propulsion based on the HJB formulation. The technique uses a dynamic model based on normalized time (true anomaly) and employs spline approximations to calculate nonintegrable input functions. These approximations allow for relatively fast calculation of single-spacecraft optimal

trajectories, which can be solved in parallel across all satellites in the cluster; the single-spacecraft optimal trajectories are then used to determine formation optimal conditions. The theoretical approach can be extended to any system in which a state transition matrix and stable initial state are known and provides an idealized basis to which perturbed closed-loop maneuvers can be compared.

The optimal formation planner was demonstrated and analyzed using a tetrahedral formation, common to several proposed satellite cluster missions. The planar, single-satellite minimum-time solutions solve for three switch times and a final time; the minimum-fuel maneuvers contain 4–6 switch times as a function of the final maneuver time. The fuel costs decrease rapidly for small increases in the final maneuver time, and the thrust profile typically acts at or near perigee of the orbit; both conclusions indicate that a smart planner such as the one proposed could save fuel in future formation-based missions. Single-satellite maneuvers can be calculated in $\approx$5–10 s, and the full formation planner can be solved in minutes using MATLAB. Because the technique is parallelizable across a cluster, calculation time for the formation optimal planner is well under an orbit for both minimum-time and minimum-fuel determinations, providing a practical alternative to current finite horizon techniques. Comparisons with LP approaches show a definitive savings in fuel for cases of high eccentricity orbits and strict requirements on endpoint accuracy.

Appendix A: State Dynamics Fundamental Matrix Solution

A complete presentation of the development of the fundamental matrix solution to the relative orbital dynamics problem outlined in Sec. II is done by Humi.[24] The solution without singularities is given by Carter.[10] This fundamental matrix solution $\Phi(\theta)$ is

$$\Phi(\theta) = \begin{bmatrix} 2S(\phi_1) & 2S(\phi_2) & S(2\phi_3+1) & 1 & 0 & 0 \\ 2\phi_1 & 2\phi_2 & 2\phi_3+1 & 0 & 0 & 0 \\ \phi_1 & \phi_2 & \phi_3 & 0 & 0 & 0 \\ \phi_1' & \phi_2' & \phi_3' & 0 & 0 & 0 \\ 0 & 0 & 0 & 0 & \cos\theta & \sin\theta \\ 0 & 0 & 0 & 0 & -\sin\theta & \cos\theta \end{bmatrix} \tag{A1}$$

where

$$\rho(\theta) = 1 + e\cos\theta$$

$$\cos E = \frac{\cos\theta + e}{1 + e\cos\theta}$$

$$\sin E = \frac{\sqrt{1-e^2}\sin\theta}{1 + e\cos\theta}$$

$$\cos\theta = \frac{\cos E - e}{1 - e\cos E}$$

$$K(\theta) = (1-e^2)^{-\frac{5}{2}}\left[\frac{1}{2}E - \frac{1}{2}\sin E\cos E - \frac{e}{3}\sin^3 E\right]$$

$$\phi_1(\theta) = \rho(\theta)\sin\theta$$

$$\phi_1'(\theta) = \cos\theta + e(\cos^2\theta - \sin^2\theta)$$

$$S[\phi_1(\theta)] = -\cos\theta\left[1 + \frac{e}{2}\cos\theta\right]$$

$$\phi_2(\theta) = -6e^2\phi_1(\theta)K(\theta) + \frac{2e\sin^2\theta}{\rho(\theta)^2} - \frac{\cos\theta}{\rho(\theta)}$$

$$\phi_2'(\theta) = -6e^2\phi_1'(\theta)K(\theta) + \frac{2e\sin\theta}{\rho(\theta)^3}(2\cos\theta - 3e\sin^2\theta + 2e) + \frac{\sin\theta}{\rho(\theta)^2}$$

$$S[\phi_2(\theta)] = 3e\rho(\theta)^2K(\theta) - \frac{\sin\theta}{\rho(\theta)}$$

$$\phi_3(\theta) = 6e\phi_1(\theta)K(\theta) - \frac{2\sin^2\theta}{\rho(\theta)^2} - \frac{\cos^2\theta}{\rho(\theta)} - \cos^2\theta$$

$$\phi_3'(\theta) = 6e\phi_1'(\theta)K(\theta) + \frac{6e\sin^3\theta}{\rho(\theta)^3} - \frac{4\sin\theta(e+\cos\theta)}{\rho(\theta)^3} + \sin\theta\cos\theta\frac{(2+e\cos\theta)}{\rho(\theta)^2} + 2\sin\theta\cos\theta$$

$$S[2\phi_3(\theta)+1] = -6\rho(\theta)^2K(\theta) - \frac{2\sin\theta\cos\theta}{\rho(\theta)} - \sin\theta\cos\theta$$

and $S(\cdot)$ is defined as

$$S(\cdot) = S[\cdot(\theta)] = \int_{\theta_0}^{\theta} \cdot(\tau)\,\mathrm{d}\tau$$

The inverse of this matrix is

$$\Phi^{-1}(\theta) = \begin{bmatrix} 0 & -2S(\phi_2) & 4S(\phi_2)+\phi_2' & -\phi_2 & 0 & 0 \\ 0 & 2S(\phi_1) & -4S(\phi_1)-\phi_1' & \phi_1 & 0 & 0 \\ 0 & 1 & -2 & 0 & 0 & 0 \\ 1 & -S(2\phi_3+1) & 2S(2\phi_3+1)+\phi_3' & -\phi_3 & 0 & 0 \\ 0 & 0 & 0 & 0 & \cos\theta & -\sin\theta \\ 0 & 0 & 0 & 0 & \sin\theta & \cos\theta \end{bmatrix} \tag{A2}$$

Appendix B: Costate Matrix Solution

The fundamental matrix solution to the costate problem can be found by the identity

$$\Psi(\theta) = \Phi^{-T}(\theta)\begin{bmatrix} 0 & -1 & 0 & 0 & 0 & 0 \\ 1 & 0 & 0 & 0 & 0 & 0 \\ 0 & 0 & 0 & 1 & 0 & 0 \\ 0 & 0 & -1 & 0 & 0 & 0 \\ 0 & 0 & 0 & 0 & 0 & -1 \\ 0 & 0 & 0 & 0 & 1 & 0 \end{bmatrix} \tag{B1}$$

with $\Phi^{-1}(\theta)$ as defined in Appendix A. The matrix $\Psi^{-1}(\theta)$ is then

$$\Psi^{-1}(\theta) = \begin{bmatrix} 0 & 1 & 0 & 0 & 0 & 0 \\ -1 & 0 & 0 & 0 & 0 & 0 \\ 0 & 0 & 0 & -1 & 0 & 0 \\ 0 & 0 & 1 & 0 & 0 & 0 \\ 0 & 0 & 0 & 0 & 0 & 1 \\ 0 & 0 & 0 & 0 & -1 & 0 \end{bmatrix}\Phi^{T}(\theta) \tag{B2}$$

where $\Phi(\theta)$ is also given in Appendix A.

Acknowledgments

This research is funded under the NASA Cross-Enterprise Technology Development Program, NASA Grant NAG5-10440.

References

[1]"The Magnetospheric Multiscale Mission: Resolving Fundamental Processes in Space Plasmas," proposal to NASA, URL: http://stp.gsfc.nasa.gov/documents/mms/mms_stdt_report.pdf [cited 7 Nov. 2005].

[2]Goddard Space Flight Center Magnetospheric Constellation, URL: http://stp.gsfc. nasa.gov/missions/mc/mc.htm [cited 2 Jan. 2004].

[3]Tsien, W., Finley, C., Mocio, M., and Olmedo, C., "Advancing Military-Relevant Space Technologies," AIAA Paper 2003-6363, 2003.

[4]Cash, W., "MAXIM Preliminary Design," proposal to NASA, 2000, URL: http://maxim.gsfc.nasa.gov/docs/mission/niacdesign.pdf [cited 27 July 2003].

[5]Campbell, M. E., "Planning Algorithm for Multiple Satellite Clusters," *Journal of Guidance, Control, and Dynamics*, Vol. 26, No. 5, 2003, pp. 770–780.

[6]Robertson, A., Inalhan, G., and How, J. P., "Spacecraft Formation Flying Control Design for the Orion Mission," AIAA Paper 99-4266, Aug. 1999.

[7]Campbell, M. E., Knagenhjelm, V., and Yingling, J., "Flight Software Development for the ION-F Formation Flying Mission," *Institute of Electrical and Electronics Engineers Aerospace Conference Proceedings*, Vol. 2, IEEE Publications, Piscataway, NJ, 2001, pp. 553–562.

[8]Scharf, D., Hadeagh, F., and Kang, B., "A Survey of Spacecraft Formation Flying: Part I, Guidance," *Proceedings of the 2003 American Control Conference*, Vol. 2, IEEE Publications, Piscataway, NJ, 2003, pp. 1733–1739.

[9]Sabol, C., Burns, R., and McLaughlin, C. A., "Satellite Formation Flying Design and Evolution," American Astronomical Society AAS Paper 99-121, 1999.

[10]Carter, T. E., "State Transition Matrices for Terminal Rendezvous Studies: Brief Survey and New Example," *Journal of Guidance, Control, and Dynamics*, Vol. 21, No. 1, 1998, pp. 148–155.

[11]Tillerson, M., and How, J. P., "Advanced Guidance Algorithms for Spacecraft Formation Flying," *Proceedings of the 2002 American Control Conference*, Vol. 4, IEEE Publications, Piscataway, NJ, 2002, pp. 2830–2835.

[12]Kumar, R., and Seywald, H., "Fuel-Optimal Stationkeeping via Differential Inclusions," *Journal of Guidance, Control, and Dynamics*, Vol. 18, No. 5, 1995, pp. 1156–1162.

[13]Tillerson, M., Inalhan, G., and How, J. P., "Coordination and Control of Distributed Spacecraft Systems Using Convex Optimization Techniques," *International Journal of Robust and Nonlinear Control*, Vol. 12, No. 2–3, 2002, pp. 207–242.

[14]Milam, M. B., Petit, N., and Murray, R. M., "Constrained Trajectory Generation for Microsatellite Formation Flying," AIAA Paper 2001-4050, Aug. 2001.

[15]Carter, T. E., and Alvarez, S. A., "Quadratic-Based Computation of Four-Impulse Optimal Rendezvous near Circular Orbit," *Journal of Guidance, Control, and Dynamics*, Vol. 23, No. 1, 2000, pp. 109–117.

[16]Gim, D., and Alfriend, K. T., "State Transition Matrix of Relative Motion for the Perturbed Non-Circular Reference Orbit," American Astronomical Society, AAS Paper 01-222, Feb. 2001.

[17]Rayburn, C., Campbell, M., and Mattick, T., "Pulsed Plasma Thruster System for Microsatellites," *Journal of Spacecraft and Rockets*, Vol. 42, No. 1, 2005, pp. 161–170.

[18]Spores, R. A., Spanjers, G., Birkan, M., and Lawrence, T., "Overview of the USAF Electric Propulsion Program," AIAA Paper 2001-3225, July 2001.

[19]Ross, "How to Find Minimum Fuel Controllers," AIAA Paper 2004-5346, Aug. 2004.

[20]Campbell, M. E., "Collision Monitoring and Avoidance in Satellite Clusters," *IEEE Transactions of Control System Technology*, Vol. 13, No. 1, 2005, pp. 42–55.

[21]Alfriend, K. T., and Schaub, H., "Dynamics and Control of Spacecraft Formations: Challenges and Some Solutions," *Advances in the Astronautical Sciences*, Vol. 106, American Astronomical Society, Univelt, Inc., San Diego, CA, 2000, pp. 205–224.

[22]Inalhan, G., Tillerson, M., and How, J. P., "Relative Dynamics and Control of Spacecraft Formations in Eccentric Orbits," *Journal of Guidance, Control, and Dynamics*, Vol. 25, No. 1, 2002, pp. 48–59.

[23]Tschauner, J., and Hempel, P., "Rendezvous zu einem in elliptischer Bahn umlaufenden Ziel," *Astronautica Acta*, Vol. 11, No. 5, 1965, pp. 104–109.

[24]Humi, M., "Fuel-Optimal Rendezvous in a General Central Force Field," *Journal of Guidance, Control, and Dynamics*, Vol. 16, No. 1, 1993, pp. 215–216.

[25]de Boor, C., *A Practical Guide to Splines*, Springer-Verlag, New York, 1978.

[26]Farin, G., *NURBS: from Projective Geometry to Practical Use*, A. K. Peters, Natick, MA, 1999.

[27]Zanon, D. J., and Campbell, M. E., "Optimal Planning for Tetrahedral Formations Near Elliptical Orbits," AIAA Paper 2004-5127, Aug. 2004.